A Robust Focusing and Astigmatism Correction Method for the Scanning Electron Microscope

K.H. Ong, J.C.H. Phang, J.T.L. Thong

Centre for Integrated Circuit Failure Analysis and Reliability (CICFAR), Faculty of Engineering, National University of Singapore, Singapore

Summary: This paper discusses a new approach to focusing and astigmatism correction based on the fast fourier transforms (FFTs) of scanning electron microscopy (SEM) images. From the FFTs, it is possible to obtain information on the severity of the defocus and astigmatism. This information is then processed by an algorithm to perform real-time focusing and astigmatism correction on the SEM. The algorithm has been tested on defocused and astigmatic images of different samples, including those with highly directional features. Experiments show that the images obtained after running the algorithm can be as good as those that an experienced SEM operator can achieve.

Key words: astigmatism correction, focusing, Fourier transforms, scanning electron microscopy, automation

Introduction

In scanning electron microscopy (SEM), focusing and astigmatism correction are crucial operations for imaging. Manual focusing and astigmatism correction is a time-consuming process and can be difficult even for an experienced SEM operator, particularly in low-dose and high-resolution work. Several attempts that have been made to automate the focusing and astigmatism correction process are discussed in the following.

Previous automatic focusing and astigmatism correction methods usually fall into one of two categories: those that determine the point of best focus and zero astigmatism from the derivative or gradient of the video signal and those that analyse the power spectrum or diffraction pattern of the signal.

One proposed digital method is based on the gradient of the image which maximizes the sum of the intensity gradient magnitudes over the whole image (Tee *et al.* 1979). Another

technique maximises the sum of the squared differences between neighbouring points in the line scan direction over the entire image (Burge *et al.* 1976).

A major disadvantage of using gradient methods is that, since they are based on differentiating the video signal, they are inherently sensitive to noise. Thus, alternative techniques based on the power spectrum have been investigated. It has been shown that it is possible to determine the resolution of an SEM accurately from the width of the power spectrum and to detect astigmatism from the asymmetry of the power spectrum (Erasmus and Smith 1982). Since the power spectrum is equal to the Fourier transform of the covariance function (CF) of an image, the CF also contains information about defocus and astigmatism. It has been shown that focusing and astigmatism correction of the SEM could be achieved using only the height of the central CF peak while ignoring its shape. The height of the central peak of the CF is simply the variance of the image. In the reported work, the complete method for automatic focusing and astigmatism correction of an SEM consists of the following steps: (1) measure the image variance versus focus curve; find the centre of symmetry of this curve and set the focus current to the central value; (2) repeat the process with the x-stigmator; (3) repeat this process with the y-stigmator. If necessary, the whole procedure is repeated to improve the accuracy of the result. The major disadvantage of this technique is that the measurement of the various curves, such as the image variance versus focus curve, requires the collection of image variances for different focus currents. This, in turn, means that the accuracy of the algorithm is limited by the number of points used to plot the curve. If too few points are plotted, the accuracy of the calculated centre of symmetry of the curve is reduced. If too many points are used, the time consumed in the data collection process lengthens. Furthermore, three curves need to be plotted, which means that the total time required for one iteration is three times that of the time taken to determine a single curve. Also, the technique is reported to operate best at a magnification of 3,000×, which is too low a magnification for high-resolution SEM work.

With the advent of faster and cheaper processors, the use of fast Fourier transform (FFT) in SEM is becoming viable. A new application of FFT is found in the area of SEM resolution evaluation (Dodson and Joy 1990, Martin *et al.* 1995). A recent work in SEM resolution evaluation discusses how FFT

---

can be used to detect defocus and astigmatism in SEM images (Postek and Vladar 1996). In the paper, a quantitative approach is employed in detecting the change in the FFT of a gold-on-carbon image as focus is varied. A figure-of-merit that is directly proportional to the high-frequency content of an image is calculated from its FFT. Among the SEM images at different focus, the figure-of-merit obtained from the FFT of the focused image is the largest. It is also observed that the distributions of the one-dimensional (1-D) FFT of a horizontal and a vertical line scan of a gold-on-carbon image are different if astigmatism is present.

Although most modern SEMs are equipped with functions for performing automatic focusing and astigmatism correction, they do not perform up to expectation for samples containing highly directional features. This paper discusses a new technique that can be used to quantify both defocus and astigmatism from the FFTs of SEM images. The information is then incorporated into an algorithm to perform automatic focusing and astigmatism correction on the SEM in real time. The algorithm has been tested to work well on a wide variety of samples, including samples with highly directional features.

Fast Fourier Transform and Scanning Electron Microscopy

It has been observed that information on the defocus and astigmatism of an SEM image can be found in its FFT. In image processing, it is well known that the amount of high-frequency components present in the FFT indicates how sharp an image is; this is because the edges and boundaries of an image are represented in the FFT by the high-frequency components. When an image is defocused, the edges and boundaries are blurred. Thus, the FFT of the image contains lesser high-frequency components than the corresponding FFT of the focused image.

Electron Lens Optics

For an astigmatic electron beam, the beam in the SEM is brought to two mutually perpendicular line foci as illustrated in Figure 1. As a result, the image experiences stretching in one of the two perpendicular directions due to the elliptical spot. The stretching is most noticeable when the image plane is close to one of the two line foci.

From the figure it is observed that when astigmatism is present, best focus is obtained when the image plane is at the position of the circular disc leading to a blurred image due to the larger spot size.

Another observation is that when the image plane is moved from overfocused to underfocused positions or vice versa, the stretching in the image suffers a 90° rotation. When focusing is performed, it can be thought of as moving the image plane up or down. When astigmatism is being corrected, it can be thought of as moving the two line foci closer together.

When an image is focused and free of astigmatism, the two line foci coincide on the image plane and the electron beam is brought to a single point giving the smallest spot size or highest possible resolution, as shown in Figure 2. At this point, the over- and underfocused images are similar, with no noticeable stretching in either of the two images.

The algorithm developed in this paper makes use of the rotation of the image "stretch" to correct astigmatism and the amount of high-frequency components in the FFTs to adjust focus.

Hardware

The SEM used in this work is a Hitachi S-4100 cold field emission (FE) instrument. The lens system is a two-stage electromagnetic lens and the stigmator is of the electromagnetic type. A DEC AlphaStation 500/400 is also being employed to control the SEM parameters and to capture and process the images.

System setup: The diagram of the closed-loop control system used for automatic focusing and astigmatism correction is shown in Figure 3. The image of the specimen is captured by a workstation via a video input card seated in the workstation. Control of the SEM is achieved by an RS232 communication link connecting the workstation to the SEM. The correction process continues until a focused and astigmatism-free image is obtained.
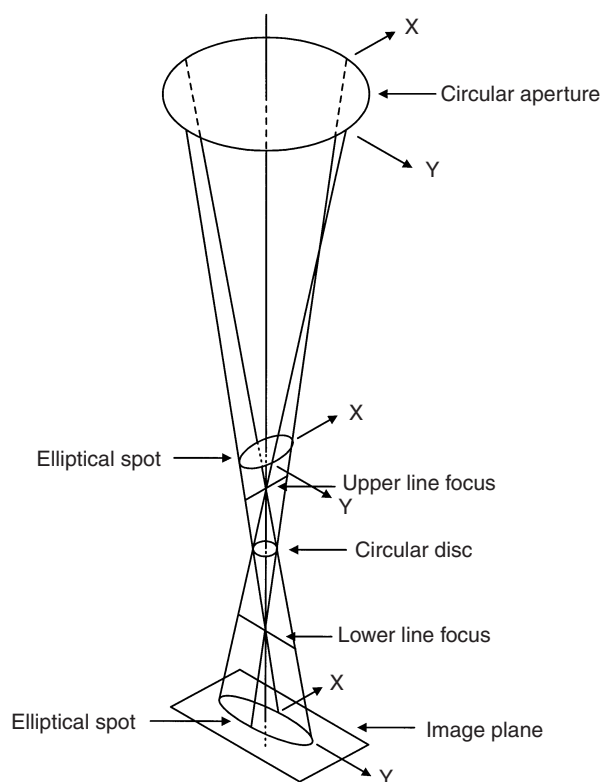

FIG. 1   Diagram illustrating the defocus and astigmatism of images.

Focusing and astigmatism correction on the SEM: In practice, the focal length of the lens is adjusted by altering the excitation of the final lens. The focus control on the SEM is used to adjust the final lens current. On the Hitachi S-4100 FESEM, the final lens current can be set through the RS232 communication link to achieve a working distance from 0 to 39 mm.

For astigmatism correction, electromagnetic stigmators are used to provide a quadrupole field to correct the beam ellipticity (Riecke 1982). A typical octopole stigmator configuration is shown in Figure 4. The same current flows through coils A1, A2, B1, and B2, while a different current flows through coils C1, C2, D1, and D2. The magnetic field generated by coils A1, A2, B1, and B2 controls the amount of stretching along the A- and B-axes. Similarly, the field generated by coils C1, C2, D1, and D2 controls the amount of stretching along C- and D-axes. The magnitude and direction of the current through coils A1, A2, B1, and B2 are controlled by the stigmator (stigma for short) x^1 control on the SEM, whereas the magnitude and direction of the current through coils C1, C2, D1, and D2 are controlled by the stigmator y^2 control. Thus, by adjusting the stigma x and y controls on the SEM, astigmatism can be corrected. The controls are adjusted through the RS232 communication link.

[1,2] Each stigmator control adjusts the magnetic field strength of an independent set of coils to correct the beam ellipticity. The two sets of coils are 45° apart as shown in Figure 4 and not orthogonal as suggested by the terms x and y.
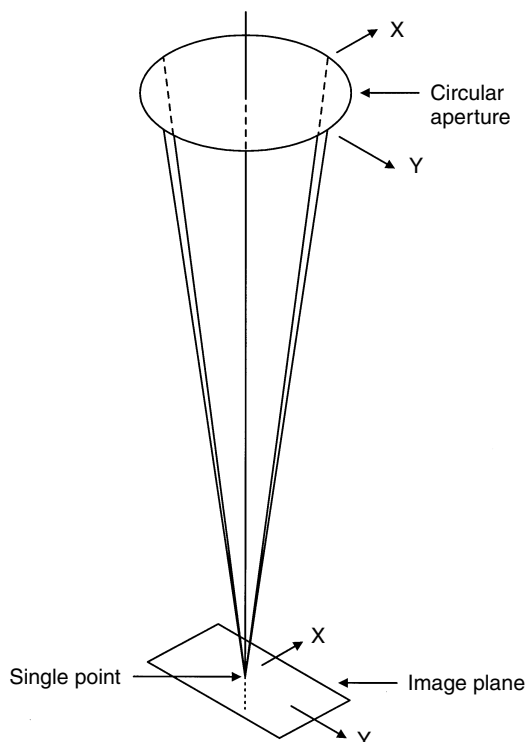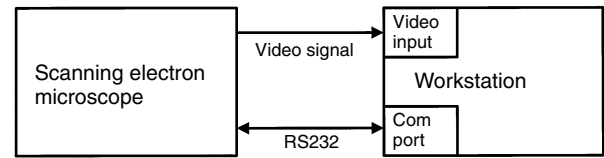

FIG. 3   Closed-loop control system used for performing automatic focusing and astigmatism correction.
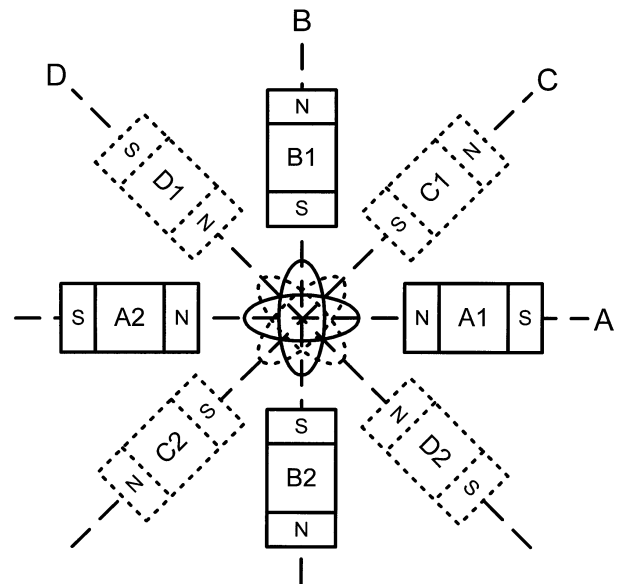
FIG. 4   A typical octopole stigmator configuration commonly used in scanning electron microscopes.

FIG. 2   Diagram illustrating the formation of a focused and astigmatism-free image.

Experimental Observations

As illustrated earlier, an SEM image experiences stretching when there is astigmatism. To characterise the stretch in the image, its FFT is used. The stretch in the FFT is orthogonal to the stretch in the image due to the nature of the Fourier transform. Figure 5 illustrates gold-on-carbon images and their corresponding FFTs for different degrees of defocus and astigmatism. The image is 256 × 256 pixels with 256 gray levels. This is found to be sufficient for analytical and correction purposes, and a larger image can always be captured after the correction has been performed by the algorithm. The gold-on-carbon sample is chosen mainly because its FFT is symmetrical and circular, which makes it easier to illustrate the principles involved in quantifying defocus and astigmatism information from the FFTs.
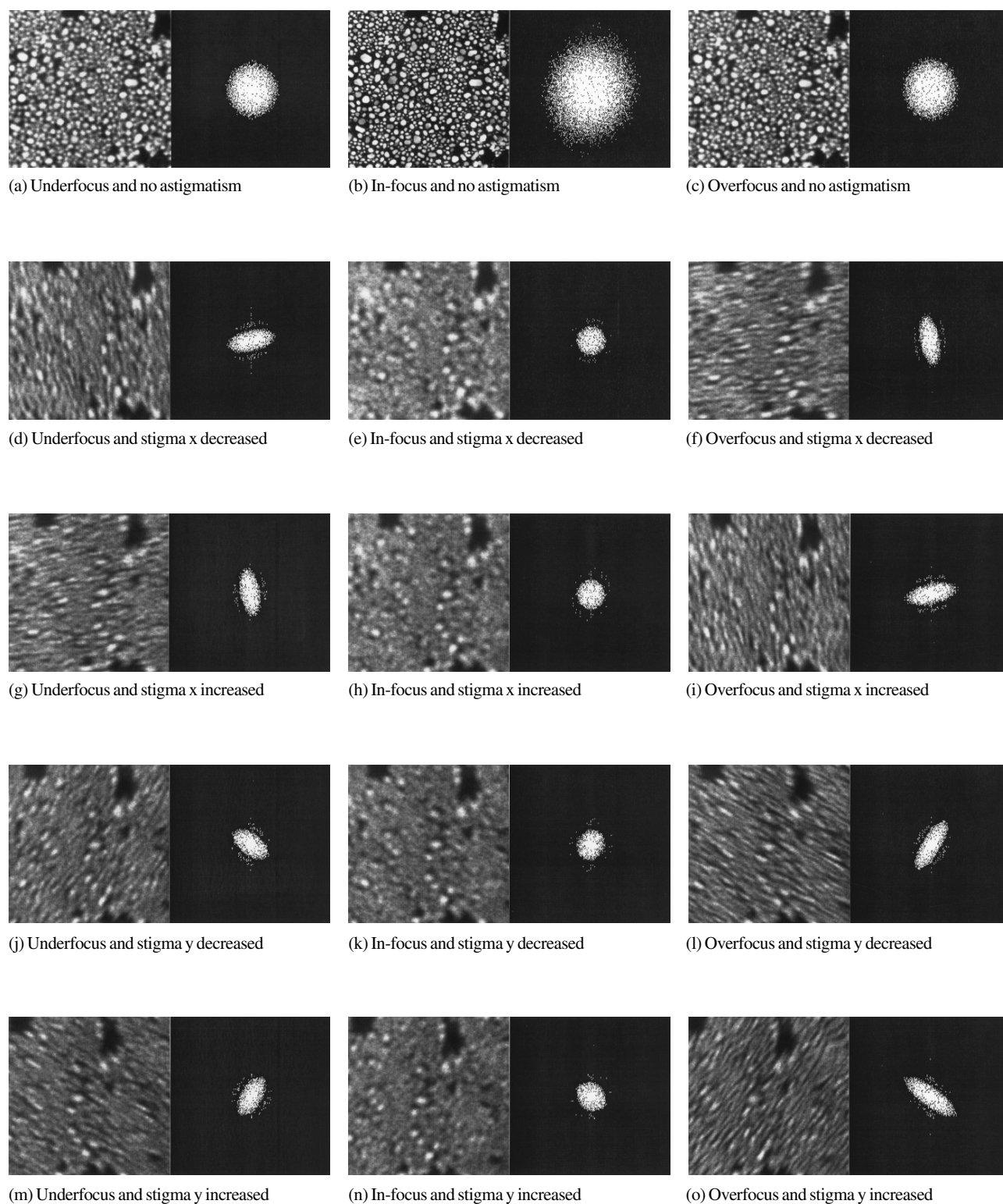
(a) Underfocus and no astigmatism

(b) In-focus and no astigmatism

(c) Overfocus and no astigmatism

(d) Underfocus and stigma x decreased

(e) In-focus and stigma x decreased

(f) Overfocus and stigma x decreased

(g) Underfocus and stigma x increased

(h) In-focus and stigma x increased

(i) Overfocus and stigma x increased

(j) Underfocus and stigma y decreased

(k) In-focus and stigma y decreased

(l) Overfocus and stigma y decreased

(m) Underfocus and stigma y increased

(n) In-focus and stigma y increased

(o) Overfocus and stigma y increased

FIG. 5   Images of gold-on-carbon sample and their fast Fourier transforms (FFTs) for different degrees of defocus and astigmatism (horizontal field width = 1.94 μm). The FFTs of the images are displayed in 256 gray levels. To have a better visualisation of the defocus and astigmatism information in the FFTs, the FFTs are threshold using a value of 90 determined experimentally. The terms "stigma x/y increased/decreased" denote that the software value of the stigma x/y control on the scanning electron microscope is increased/decreased with respect to the value that causes the image to be free of astigmatism. The over- and underfocused images are obtained by decreasing or increasing focal length, respectively.

Algorithm Development

Based on the observations in Figure 5, an algorithm is developed to correct focus and astigmatism based on the FFTs of the images. Figure 6 gives the general flow chart of the algorithm developed to perform automatic focusing and astigmatism correction.

The algorithm begins by storing the focus and stigma values of the SEM. Next, the algorithm offsets the focus of the SEM to capture the over- and underfocused images. The FFTs of these images are calculated and compared. If the two FFTs are similar, the algorithm stops. Otherwise, it adjusts the focus and stigmator values of the SEM accordingly. This en-

tire process is repeated until a focused and astigmatism-free image is obtained. Notice that it is possible that the algorithm adjusts neither the focus nor the stigma values in an iteration. This occurs when astigmatism in the SEM is almost corrected and image noise masks out the astigmatism information in the FFTs. In such cases, the algorithm ignores the FFTs and recaptures the over- and underfocused images. Typically, this occurs only once or twice in a correction process.
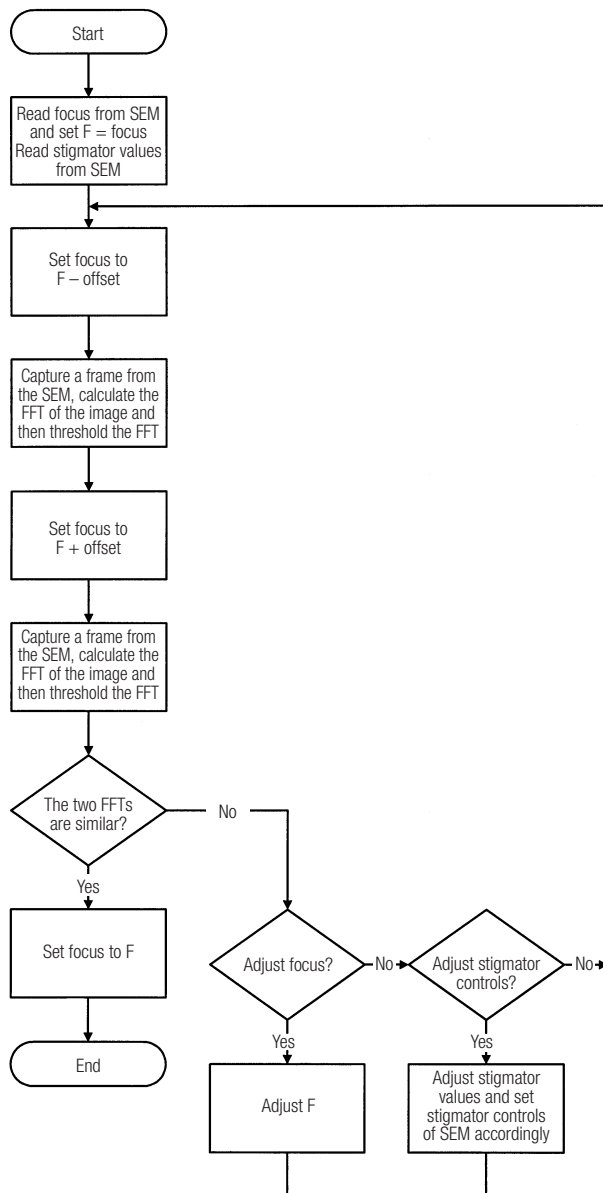
When the FFTs of the over- and underfocused images are similar, the corresponding images are also similar. This indicates that astigmatism has been corrected since the presence of astigmatism results in the FFT of the overfocused image being orthogonal to the FFT of the underfocused image [compare Fig. 5 (d) with (f), Fig. 5 (g) with (i), Fig. 5 (j) with (l), Fig. 5 (m) with (o)] .

Samples such as integrated circuit (IC) tracks have highly directional features such as lines and squares. These features mask out important information on defocus and astigmatism in the FFTs. This technique resolves the problem by extracting defocus and astigmatism information from the comparison of the FFTs of over- and underfocused images. Furthermore, the FFT is segmented into eight regions to facilitate the quantification of defocus and astigmatism information. Thus, the algorithm can be used with a wide range of samples, including those with highly directional features. The next section discusses how defocus and astigmatism are determined from the FFTs.

Theory

The FFT is an important transform in image processing; the theory is easily found in many image processing texts (e.g., Gonzalez and Woods (1993) and it will not be discussed here.

The FFT of an image has a range of values that usually exceeds the capability of the display device. To compress the dynamic range for display and further processing, the intensity of each pixel of the FFT is transformed using the equation

$$s = c \log(1 + |r|) \tag{1}$$

where c is a scaling constant, r is the intensity of a pixel of the FFT, and s is the new value of the pixel. Using this transformation, the FFT of an image can be made to have values in the range (0, 255). This allows the FFT of an image to be displayed on the screen without loss of important information with 256 gray levels.

The most important information in the FFT of an image is at the centre of the FFT. The pixels in this central region usually have higher intensities (i.e., brighter) compared with the rest of the pixels. To extract this information more easily, the FFT is threshold with a certain value. This value is arbitrary and a value of 90 is determined experimentally to be the most suitable for this work. Thus, the FFT images throughout this paper have been threshold using a value of 90, that is, pixels with intensities ≥ 90 are displayed as white (intensity 255)

FIG. 6   General flow chart of the algorithm. SEM = scanning electron microscope, FFT = fast Fourier transform.

and pixels having intensities < 90 are displayed as black (intensity 0).

The sharpness of an image can be quantified by the number of points present in the threshold FFT. This means that the number of points present in the threshold FFT increases as the sharpness of the image improves. Let the number of points present in the threshold FFT of the over- and underfocused images be P_{of} and P_{uf} respectively. Thus, P_{of} and P_{uf} represent the sharpness of the over- and underfocused images, respectively.

To quantify the amount of astigmatism present in the image, the threshold FFT is segmented, as shown in Figure 7. Regions R1–R4 represent regions of the FFT that are associated with astigmatism along the A- and B-axes, whereas regions S1–S4 are associated with astigmatism along the C- and D-axes. The A-, B-, C-, and D-axes are defined in Figure 4. Each of these regions is a segment with an angle of 45°.

Let P_{R12-of} be the percentage of points in regions R1 and R2 of the threshold FFT of the overfocused image, and P_{R34-of} be the percentage of points in regions R3 and R4 of the threshold FFT of the overfocused image. Similarly, let P_{S12-of} be the percentage of points in regions S1 and S2 of the threshold FFT of the overfocused image and P_{S34-of} be the percentage of points in regions S3 and S4 of the threshold FFT of the overfocused image. For the underfocused image, the four variables P_{R12-uf}, P_{R34-uf}, P_{S12-uf}, and P_{S34-uf} defined in a similar manner.

The percentages are calculated by dividing the number of points present in the respective regions by the total number of points in the threshold FFT and then multiplying the result by 100. Normalisation allows the algorithm to compare the two FFTs even when the number of points in the two FFTs are different.

Differences in the two FFTs are quantified by the following variables.

$$R = \frac{P_{of} - P_{uf}}{P_{of} + P_{uf}} \tag{2}$$

$$\tag{3}$$

$$\Delta_{R12} = P_{R12-of} - P_{R12-uf} \tag{4}$$

$$\Delta_{R34} = P_{R34-of} - P_{R34-uf}$$

$$\Delta_{S12} = P_{S12-of} - P_{S12-uf} \tag{5}$$

$$\Delta_{S34} = P_{S34-of} - P_{S34-uf} \tag{6}$$

Since there is a 90° rotation in the stretch present in an image as it goes from over- to underfocus, the corresponding FFTs also experience a 90° rotation. This means that (refer to Fig. 5)

1. regions R1 and R2 for the overfocused image have characteristics similar to regions R3 and R4 for the underfocused image
2. regions R3 and R4 for the overfocused image have characteristics similar to regions R1 and R2 for the underfocused image

3. regions S1 and S2 for the overfocused image have characteristics similar to regions S3 and S4 for the underfocused image
4. regions S3 and S4 for the overfocused image have characteristics similar to regions S1 and S2 for the underfocused image.

Therefore, the astigmatism along the A- and B-axes and that along the C- and D-axes is quantified by the variables A_x and A_y respectively, where

$$A_x = \left| \left(\Delta_{R12} - \Delta_{R34} \right) \div 2 \right| \tag{7}$$

$$A_y = \left| \left(\Delta_{S12} - \Delta_{S34} \right) \div 2 \right| \tag{8}$$

The factor of 2 is meant for normalisation so that the values lie between 0 and 100%. The subscript x denotes astigmatism that can be corrected by adjusting the stigma x control, whereas the subscript y denotes astigmatism that can be corrected by adjusting the stigma y control. Experimental results show that

1. when $R > 0$ the overfocused image is sharper than the underfocused image, which implies that the *focal length should be decreased.*
2. when $R < 0$ the underfocused image is sharper than the overfocused image, which implies that the *focal length should be increased.*
3. when $\Delta_{R12} > 0$ and $\Delta_{R34} < 0$ there is astigmatism along the A- and B-axes and *stigma x should be decreased*
4. when $\Delta_{R12} < 0$ and $\Delta_{R34} > 0$ there is astigmatism along the A- and B- axes and *stigma x should be increased*
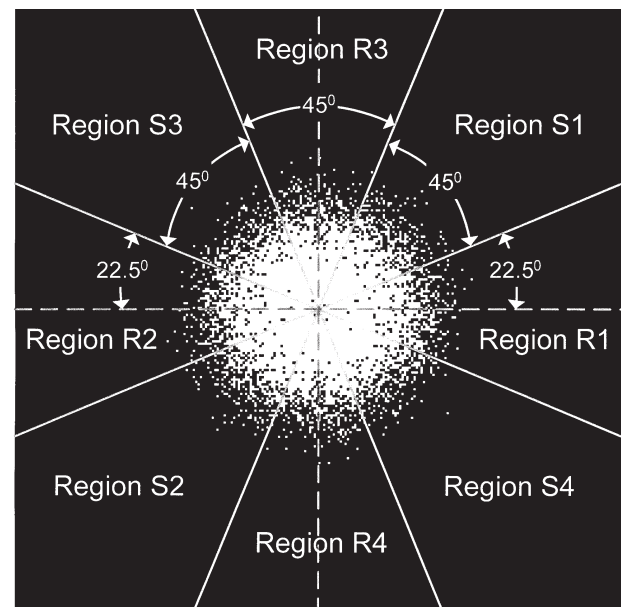

FIG. 7   Segmented fast Fourier transform.

5. when $\Delta_{S12} > 0$ and $\Delta_{S34} < 0$ there is astigmatism along the C- and D-axes and *stigma y should be increased*
6. when $\Delta_{S12} < 0$ and $\Delta_{S34} > 0$ there is astigmatism along the C- and D-axes and *stigma y should be decreased*.

The values of the variables A_x and A_y indicate whether astigmatism is more severe along the A- and B-axes or along the C- and D-axes. This allows the algorithm to correct the more severe astigmatism first.

Implementation

Using the variables defined earlier, an algorithm is developed to perform real-time focusing and astigmatism correction. Detailed flowcharts are shown in Figure 8.

The algorithm starts by reading the magnification and working distance of the SEM from which it calculates the offset required in the defocusing. Using this offset, the algorithm defocuses the SEM to capture the under- and overfocused images. The FFTs of these images are calculated and processed to extract defocus and astigmatism information. If the defocus exceeds a certain threshold, the algorithm adjusts the focus of the SEM. Otherwise, it determines the severity of the astigmatism along the A-, B-axes and C-, D-axes from which it corrects the more severe astigmatism first. The algorithm terminates when the under- and overfocused images are similar.

The variables t_1, t_1, t_1, t_1, *focus_offset, focus_step_size* and *stigma_step_size* that appear in Figure 8 can be adjusted to customise the algorithm to achieve better results.

Results

The algorithm has been tested on a wide variety of samples ranging from gold-on-carbon to IC tracks. The results show that the algorithm is robust and effective in obtaining a focused and astigmatism-free image.

Gold-on-Carbon

Figures 9 and 10 show some gold-on-carbon images before and after running the algorithm. For this experiment, t_1 is set to 90, t_2 to 0.08, t_3 to 2, and t_4 to 1. These values have been determined experimentally and have been found to work well for most samples. The focal length of the final lens is 15 mm. The variable *focus_offset* is chosen to be 10, which gives approximately a 0.1% change in the focal length. The variables *focus_step_size* and *stigma_step_size* have also been made to vary proportionally to $|R|$ and A_x (or A_y if the algorithm is correcting astigmatism along the C- and D-axes), respectively, to allow the algorithm to iterate faster to the point of best focus and zero astigmatism.

The algorithm is found to be effective in correcting defocused and astigmatic images. The values of the focus and stigma associated with the adjusted images are close to the corresponding values associated with images corrected by a human operator.

The average time taken to correct a single defocused and astigmatic image is about 2 min, with the bulk of the time spent on the communication protocol with the SEM. To set a single SEM parameter, an average time of about 1.2 s is needed. To reduce impulse noise in the captured images, median filtering is employed to preprocess the images before calculating their FFTs. The actual total computation time (this includes the time taken to median-filter the images, calculate the FFTs, and process the FFTs to extract defocus and astigmatism information) is about 12% of the total time taken for a typical correction process. This works out to be about 15 s for a 2 min correction process. If the RS232 communications with the SEM is bypassed with a direct interface to the SEM lens and stigmator drivers, the limiting time is thus typically 15 s, and this can be further reduced by optimising the computer code.

Figure 11 shows how the focus and stigma values change as the algorithm corrects the image in Figure 9(a). The upper and lower limits of the optimal values denote the range of values whereby images resulting from using any of these values are perceived to be the same by the human eye. It is observed that the corrected focus and stigma values fall within the respective optimal regions.

Integrated Circuit Tracks

Figures 12 and 13 show images of IC tracks before and after running the algorithm. For this experiment, the values of the adjustable parameters t_1, t_2, t_3, t_4, are the same as those in the previous experiment. However, the value of *focus_offset* is now set to 100, which gives an approximate 1% change in the focal length of the final lens. In this experiment, the magnification used is 4,500×. Thus, the percentage change in the focal length is chosen to be approximately 10 times higher than that in the previous experiment where the magnification is 40,000×. In SEM, the depth of field of an electron lens is the axial distance over which the lens may be focused without a perceptible change in the image sharpness. At low magnification, the depth of field can be much larger than that at higher magnification. Thus, a larger percentage change in the focal length is needed at low magnification to show any distortion in the image due to defocus and astigmatism.

From the experiment it is observed that the algorithm is able to perform equally well on samples containing highly directional features such as lines. This shows that the algorithm is robust, as it is still able to extract astigmatism information from the FFTs of samples containing highly directional features despite the fact that the FFTs are non-symmetrical and contain directional patterns. The ability of the algorithm to correct astigmatism on samples containing highly directional features is crucial since even human SEM operators have difficulty in correcting the astigmatism of these samples manually.

Figure 14 shows how the focus and stigma values change as the algorithm corrects the image in Figure 12(a). Again, the corrected values fall within the respective optimal regions.
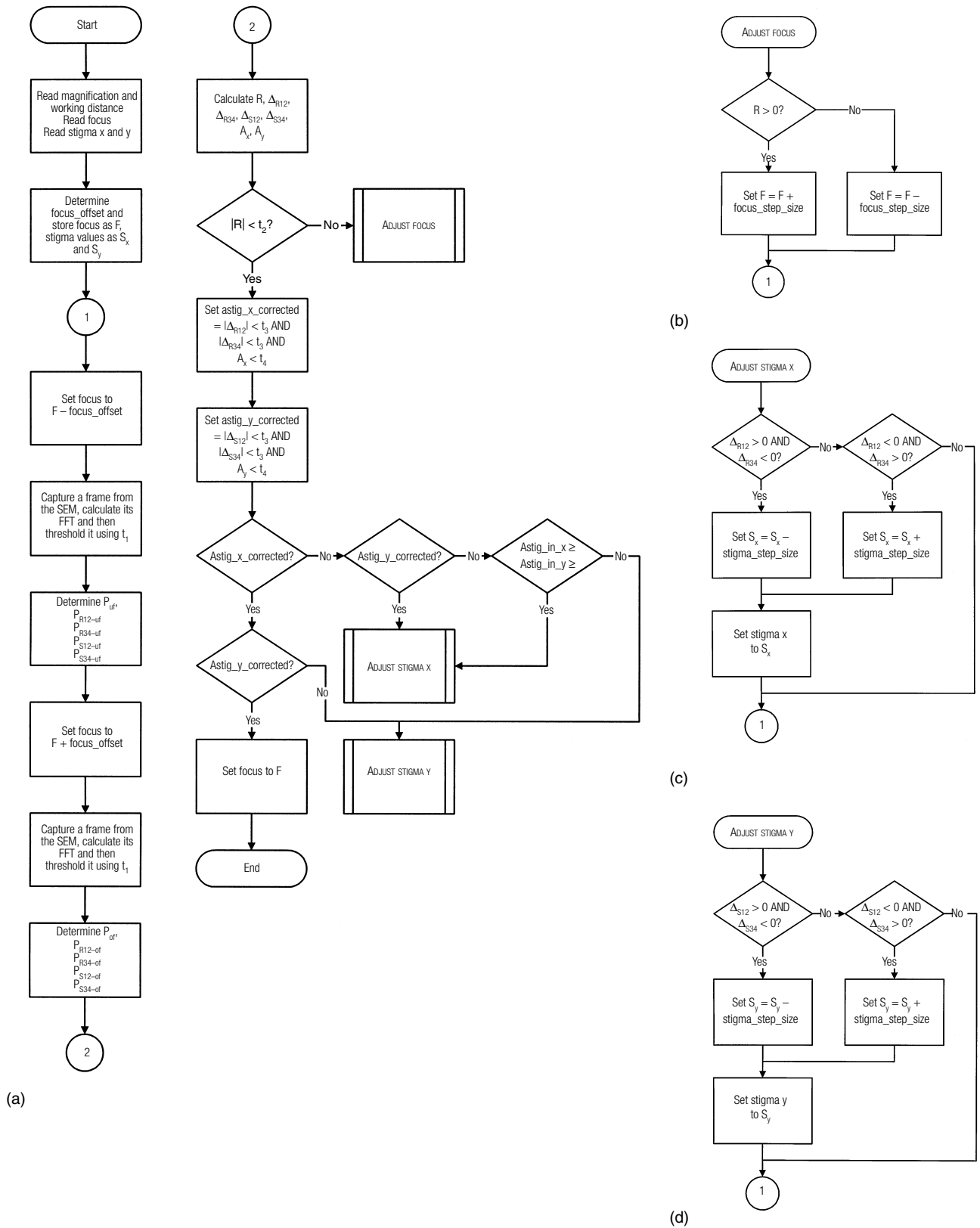
FIG. 8   Detailed flow charts of the algorithm. The terms "set focus" and "set stigma x/y" represent the sending of commands to the scanning electron microscope to change the focal length of the final lens and the magnitudes and directions of the stigmator currents, respectively. (a) Main flow chart. (b) ADJUST FOCUS subroutine. (c) ADJUST STIGMA x subroutine. (d) Adjust stigma y subroutine.
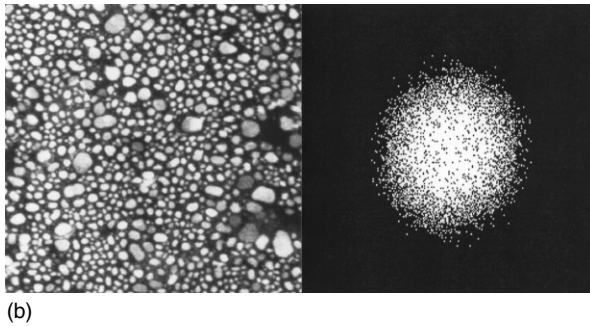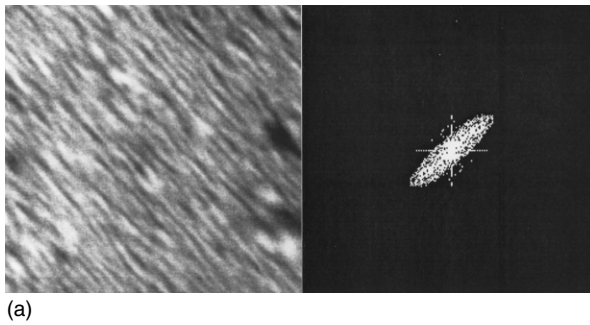
(a)

(b)

FIG. 9 An example of gold-on-carbon images (horizontal field width = 1.94 μm) obtained before and after running the algorithm and their corresponding fast Fourier transforms (FFTs). (a) A defocused and astigmatic image with its FFT. The original values of the focus, stigma x and stigma y, are 9204, 2130, and 2107, respectively. After introducing defocus and astigmatism, the new values of the focus, stigma x and stigma y, are 9190, 2000, and 2300, respectively. (b) Image obtained after running the algorithm and its corresponding FFT. Values of the focus, stigma x and stigma y, are 9203, 2126, and 2110, respectively. The time for the run is 1 min 54 s.

(a)

(b)
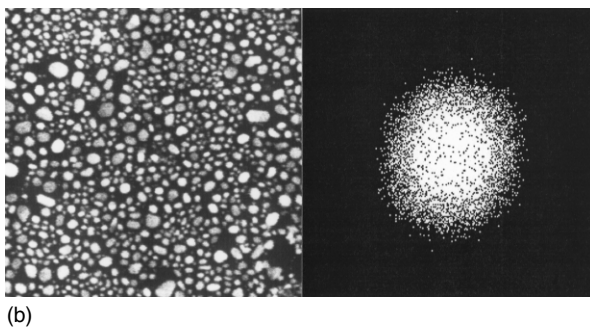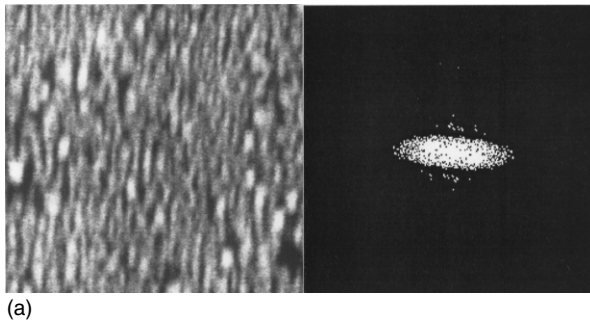
FIG. 10 Another example of gold-on-carbon images (horizontal field width = 1.94 μm) obtained before and after running the algorithm and their corresponding fast Fourier transforms (FFTs). (a) A defocused and astigmatic images with its FFT. (b) Image obtained after running the algorithm and its corresponding FFT. The time for the run is 2 min 6 s.
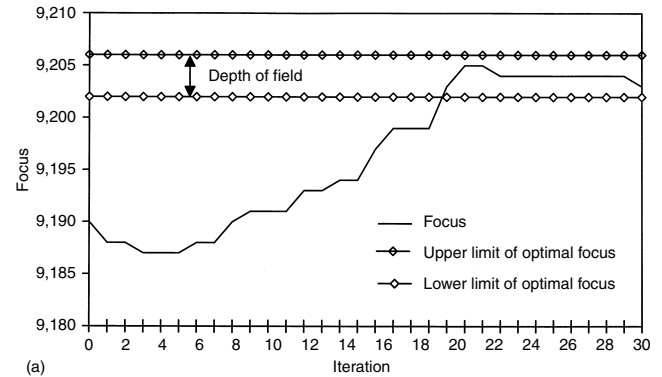

(a)

(b)

(c)
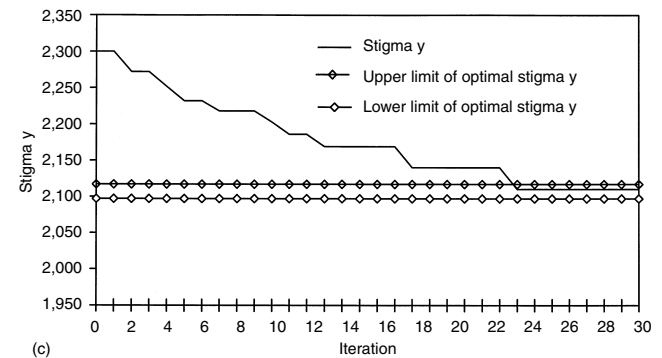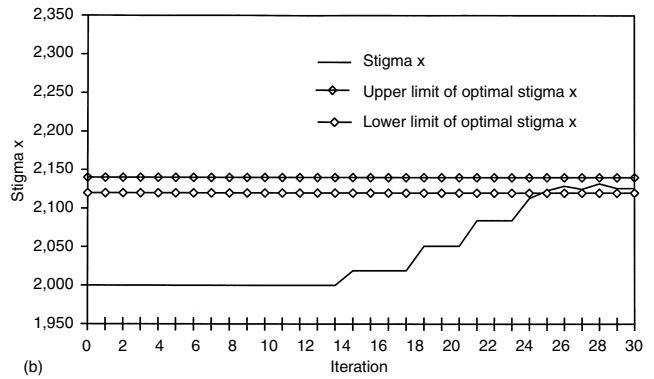
FIG. 11 Various plots obtained when the algorithm is run to correct the image in Figure 9 (a). (a) Plot of focus against iteration, (b) plot of stigma x against iteration, (c) plot of stigma y against iteration.

Other Samples

For further verification of the robustness of the algorithm, three other samples are used to test the algorithm. The first sample is a section of a hard disk platter, the second sample is silver paint, and the third sample contains IC tracks (which is the sample used in Fig. 12 but observed at a higher magnification). Figure 15 shows the images obtained before and after running the algorithm. Although there are limited features on the hard disk platter sample, the algorithm is still able to obtain a focused and astigmatism-free image.
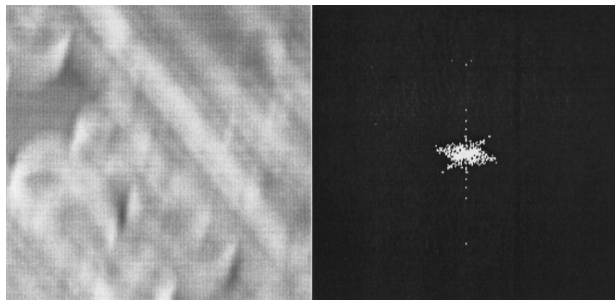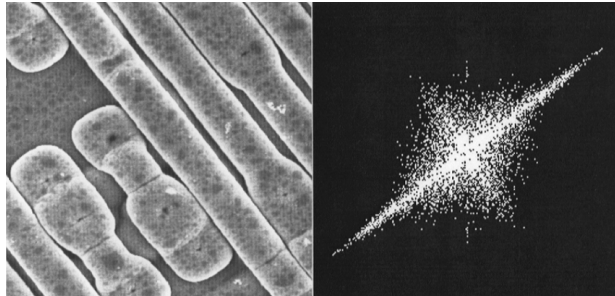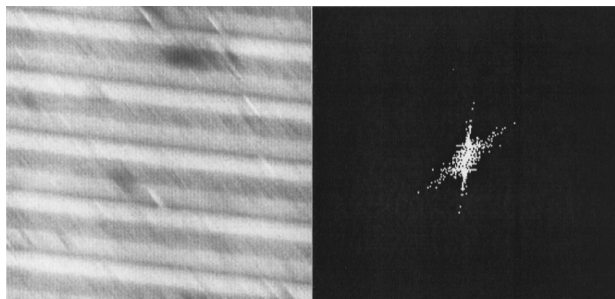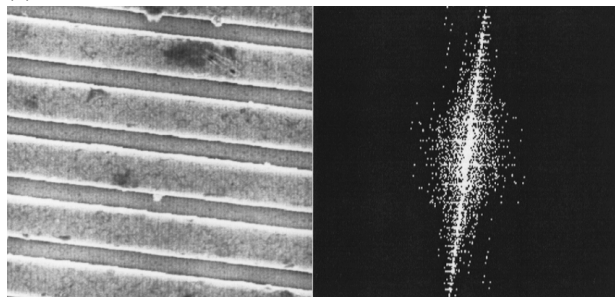
FIG. 12   An example of images of integrated circuit tracks (horizontal field width = 17.3 μm) obtained before and after running the algorithm and their corresponding fast Fourier transforms (FFTs). (a) A defocused and astigmatic image with its FFT. The original values of the focus, stigma x and stigma y, are 7265, 2105, and 2125, respectively. After introducing defocus and astigmatism, the new values of the focus, stigma x and stigma y, are 7500, 3000, and 3000, respectively. (b) Image obtained after running the algorithm and its corresponding FFT. Values of the focus, stigma x and stigma y, are 7254, 2099, and 2159, respectively. The time for the run is 2 min 33 s.
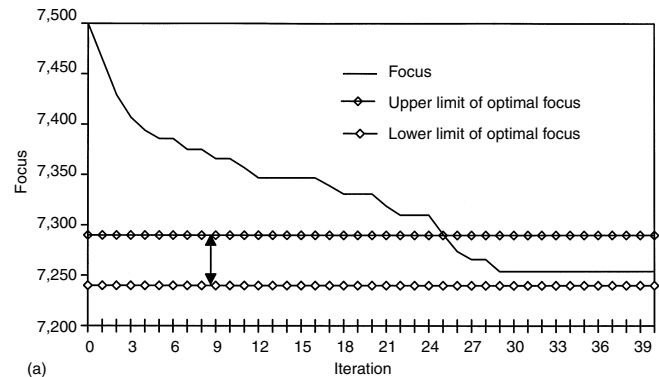

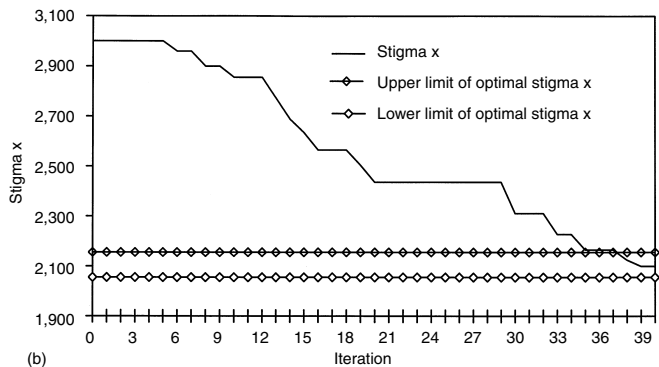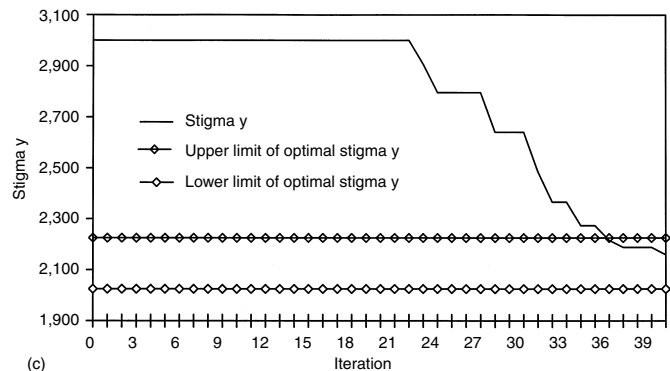FIG. 13   Another example of images of integrated circuit tracks (horizontal field width = 17.3 μm) obtained before and after running the algorithm and their corresponding fast Fourier transforms (FFTs). (a) A defocused and astigmatic image with its FFT. (b) Image obtained after running the algorithm and its corresponding FFT. The time for the run is 2 min 49 s.

FIG. 14   Various plots obtained when the algorithm is run to correct the image in Figure 12 (a). (a) Plot of focus against iteration, (b) plot of stigma x against iteration, (c) plot of stigma y against iteration.

Conclusions

A new algorithm has been developed to quantify defocus and astigmatism by comparing the FFTs of over- and underfocused images. The algorithm has been tested on a wide variety of samples and is found to be very effective in performing automatic focusing and astigmatism correction.

At high magnification, the FFTs of the images might contain too little information for the algorithm to work if there is too much defocus and astigmatism. The current solution is to start at low magnification and to repeat the algorithm with increasing magnification until the desired magnification is reached. Future work might involve the use of dynamic
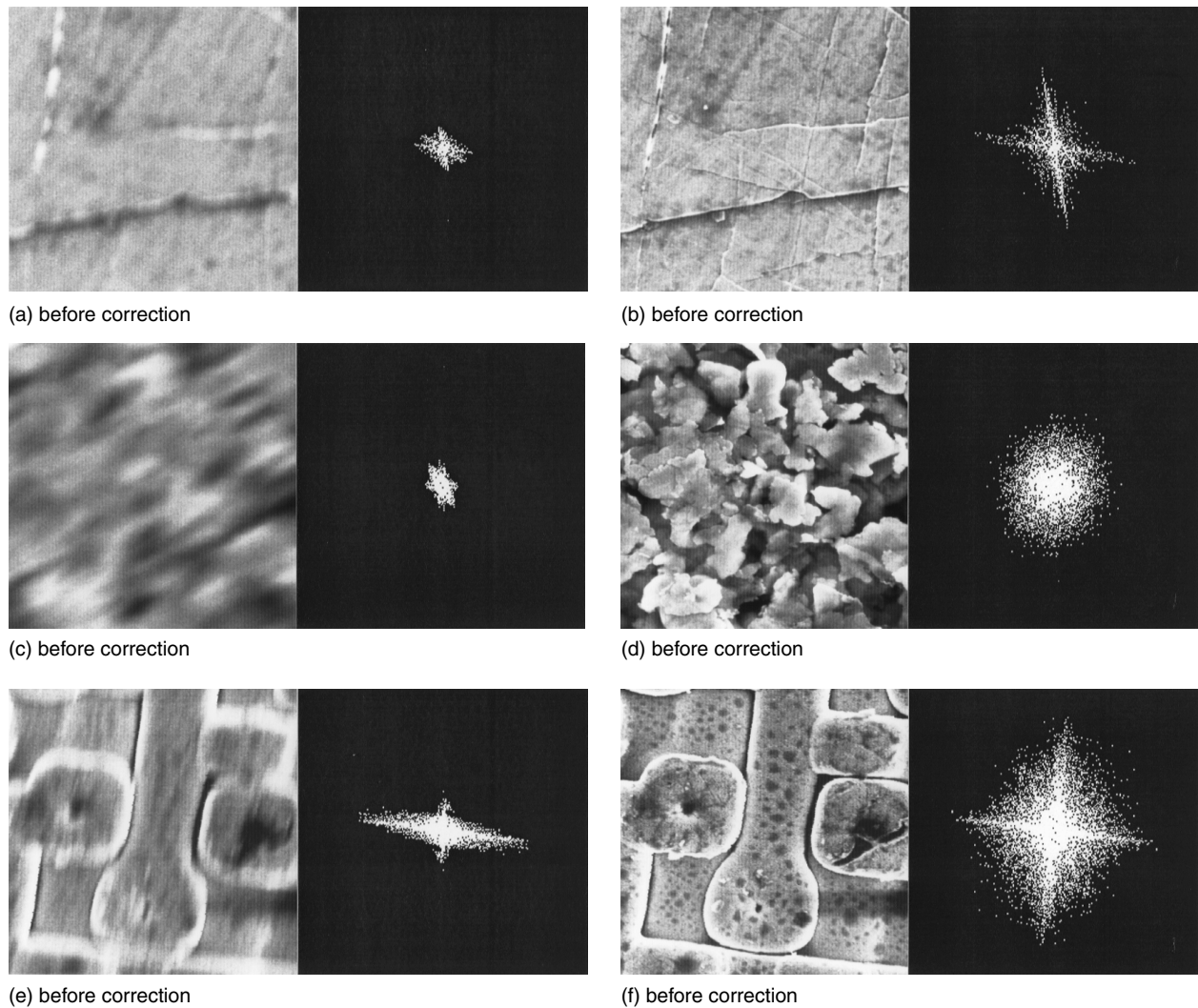
(a) before correction

(b) before correction

(c) before correction

(d) before correction

(e) before correction

(f) before correction

F$_{IG.}$ 15   Some other images obtained before and after running the algorithm. The sample in (a) and (b) is a section of a hard disk platter (horizontal field width = 31.1 µm), the sample in (c) and (d) is silver paint (horizontal field width = 5.18 µm), and the sample in (e) and (f) is integrated circuit tracks (horizontal field width = 9.72 µm). The time for the three runs is 1 min 20 s, 1 min 59 s, and 1 min 30 s, respectively.

threshold and focus offset so that the algorithm can work effectively at all magnifications. Also, the communication between the workstation and the SEM can be improved to reduce the time taken for the correction process.

Acknowledgments

References

Burge RE, Browne MT, Dainty JC, Derome M, Lackovic S: High resolution with STEM. *Proc 6th Europ Congr Electron Microscopy, Jerusalem* 1, 442–444 (1976)

Dodson TA, Joy DC: Fast Fourier transform techniques for measuring SEM resolution. *Proc XIIth Int Congr for EM*, San Francisco Press (1990) 406-407

Erasmus SJ, Smith KCA: An automatic focusing and astigmatism correction system for the SEM and CTEM. *J Microsc* 127, 185–199 (1982)

Gonzalez RC, Woods RE: *Digital Image Processing*. Addison-Wesley Publishing Co. (1993) 81–128

Martin H, Perret P, Desplat C, Reisse P: New approach in scanning electron microscope resolution evaluation. *SPIE Proc* 2439, 310–317 (1995)

Postek MT, Vladar AE: SEM performance evaluation using the sharpness criterion. *SPIE Proc* 2725, 504–514 (1996)

Riecke WD: Practical lens design. *Topics in Current Physics: Magnetic Electron Lenses*. Spring-Verlag, New York (1982) 164–351

Tee WJ, Smith KCA, Holburn DM: An automatic focusing and stigmating system for the SEM. *J Phys E: Sci Instrum* 12, 35–38 (1979)